PRAMANA
— journal of
physics

Vol. 57, Nos 2 & 3
Aug. & Sept. 2001
pp. 399–416

Meson production in $p+d$ reactions

H MACHNER*
Representing the GEM Collaboration

M Betigeri[i], J Bojowald[a], A Budzanowski[d], A Chatterjee[i], J Ernst[g], L Freindl[d], D Frekers[h], W Garske[h], K Grewer[h], A Hamacher[a], J Ilieva[a,e], L Jarczyk[c], K Kilian[a], S Kliczewski[d], W Klimala[a,c], D Kolev[f], T Kutsarova[e], J Lieb[j], H Machner[a], A Magiera[c], H Nann[a,l], L Pentchev[e], H S Plendl[k], D Protić[a], B Razen[a,g], P Von Rossen[a], B J Roy[i], R Siudak[d], J Smyrski[c], R V Srikantiah[i], A Strzałkowski[c], R Tsenov[f] and K Zwoll[b]

*Institut für Kernphysik, Forschungszentrum Jülich, 52425 Jülich, Germany
[a]Institut für Kernphysik, Forschungszentrum Jülich, Jülich, Germany
[b] Zentrallabor für Elektronik, Forschungszentrum Jülich, Jülich, Germany
[c] Institute of Physics, Jagellonian University, Krakow, Poland
[d]Institute of Nuclear Physics, Krakow, Poland
[e]Institute of Nuclear Physics and Nuclear Energy, Sofia, Bulgaria
[f]Physics Faculty, University of Sofia, Sofia, Bulgaria
[g]Institut für Strahlen- und Kernphysik der Universität Bonn, Bonn, Germany
[h]Institut für Kernphysik, Universität Münster, Münster, Germany
[i]Nuclear Physics Division, BARC, Bombay, India
[j]Physics Department, George Mason University, Fairfax, Virginia, USA
[k]Physics Department, Florida State University, Tallahassee, Florida, USA
[l]On leave from IUCF, Bloomington, Indiana, USA
Email: h.machner@fz-juelich.de

Abstract. Total and differential cross sections for the reactions $p+d \to {}^3\mathrm{He} + m^0$ with $m = \pi, \eta$ and $p + d \to {}^3\mathrm{H}+\pi^+$ were measured with the GEM detector at COSY for beam momenta between threshold and the maximum of the corresponding baryon resonance. For both reactions a strong forward–backward asymmetry was found. The data were compared with model calculations. The aspect of isospin symmetry breaking is studied.

Keywords. GEM; COSY; meson production.

PACS Nos 24.80.+y; 25.10.+s

1. Introduction

The deuteron is a loosely bound system with large distance between the two nucleons. It seems therefore a good testing ground for the impulse approximation. In addition, its wave

function as well as those of the produced light nuclei are believed to be well known and one can hope that a theoretical treatment in the three nucleon sector might be possible.

2. Kinematical aspects

Meson production in $p + d \rightarrow {}^3\mathrm{He} +$ meson reactions can occur either by the direct radiation of mesons by the nucleons or the excitation of nucleonic resonances in the intermediate state. Figure 1 shows the threshold beam energies of the protons to produce some of the resonances. Also shown are the threshold for neutral meson and two charged pion production (the meson masses are given in the right hand Y-axis of the figure). All these beam energies lie in the range available from the COSY accelerator, Juelich. For almost all of the resonances above two pion threshold one of the stongest decay mode is a nucleon plus two pions. Decay through an intermediate '$\Delta+$ pion' state is also possible with a subsequent decay of Δ into $N\pi$. The resonance $N*(S11)$ with a mass equal to 1535 MeV is the only resonance that has a strong branching ratio for the ηN channel and therefore strongly influences the reaction mechanism of eta production near threshold. We have studied the reaction mechanism of meson production in the range of above two ($\Delta(1232)$ and $N*(1535)$) resonances.

In the reactions of interest one is dealing with large momentum transfers. This is shown in figure 2 for the reactions with the neutral mesons. While the momentum transfer for the

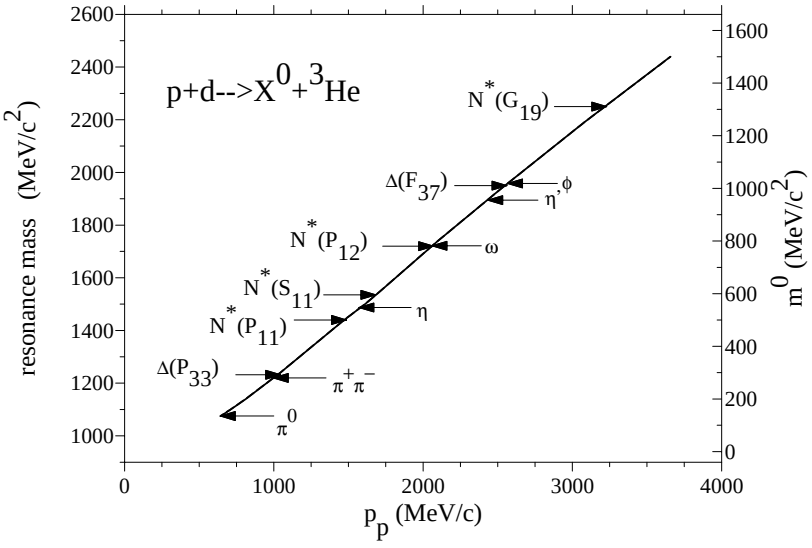

Figure 1. Excitation of baryon resonances as function of the proton beam momentum for the indicated meson. Also shown are the thresholds for neutral meson production. Some selected resonances and mesons are indicated.

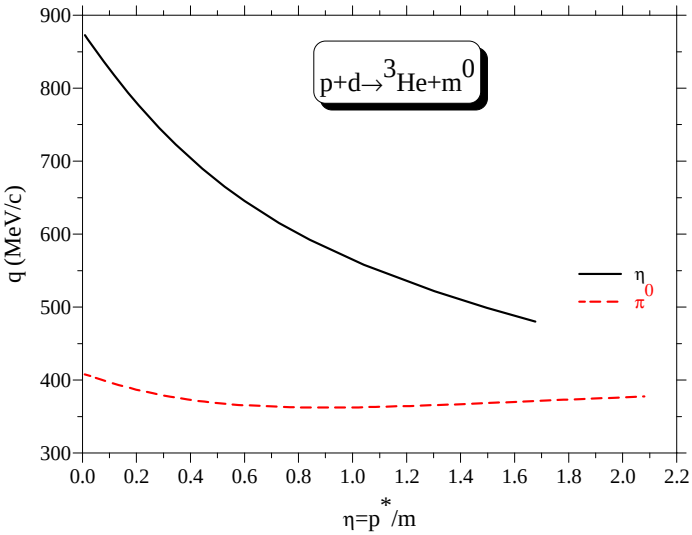

Figure 2. The momentum transfer q as function of the meson relative centre of mass momentum η.

$p + d \rightarrow {}^3$He $+\eta$ decreases strongly with increasing beam momentum, the dependence of q in the case of $p + d \rightarrow {}^3$He $+\pi^0$ reaction is rather weak. From the numbers involved one can estimate that pion production can occur on one target nucleon, whereas the large momentum transfer in the case of η-production makes such a mechanism unlikely. Both target nucleons have to participate making two step processes very likely.

The attempts for a theoretical description of the $p + d \rightarrow (A = 3)+$ meson reaction have not been particularly successful although a lot of effort was devoted to this subject over the years [1].

3. Experiments

The proton beams were extracted from the cooler-synchrotron COSY in Jülich. Although the beam was not cooled it had typically emittance of 2.5π mm mrad in all directions. The detector used is a stack of diodes made from high purity germanium (see figure 3).

The diodes have structures on the front side as well as on the rear side allowing track reconstruction, energy measurement and particle identification. With this detector called germanium wall [2], we measured the heavy $A = 3$ recoils. It allows to measure the particle type, the energy of the recoil and its direction. Thus the four momentum vector of the reaction product can be constructed. Then, by making use of conservation laws the four momentum vectors of the unobserved mesons could be extracted. Recoils being emitted under zero degree in the laboratory were measured with the magnetic spectrograph BIG KARL [3]. Both detector elements together form the GEM detector.

4. Results

In figure 4 the missing mass spectrum for charged pions from the $pd \rightarrow {}^3\mathrm{H}\pi^+$ reaction at 850 MeV/c is shown. Two things are worth mentioning: the high statistics in the

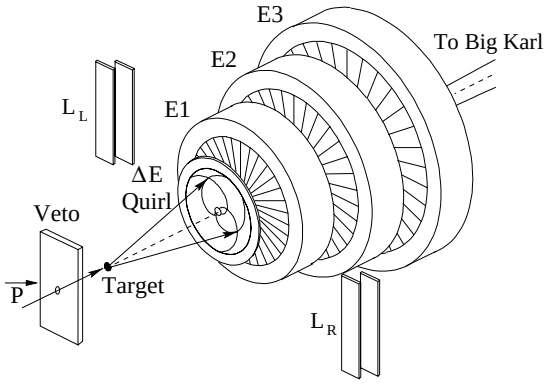

Figure 3. The germanium wall. The response of the Quirl detector to a two hit event is shown. To the left and right there are two luminosity monitors, consisting of two scintillator paddles each. Each pair acts in coincidence and is denoted by L_R and L_L, respectively.

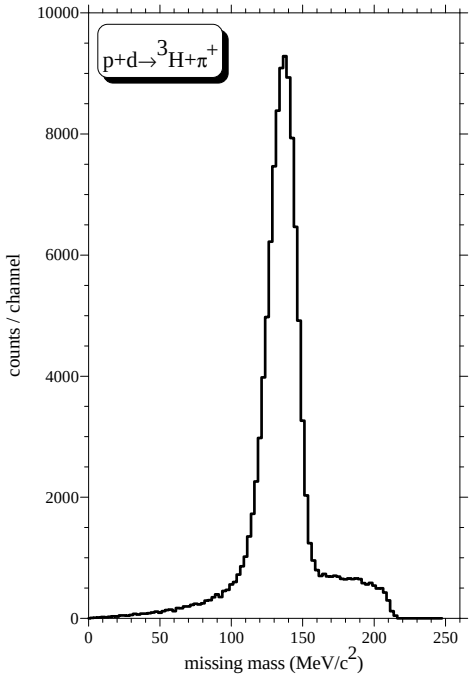

Figure 4. Deduced missing mass for the charged pion from the kinematical complete measurement of the triton. The small background was subtracted for each angular bin.

experiment and the small background. In case of the η production the background is larger due to multi-pion production. The background was subtracted by fitting a smooth curve to it. The resulting counting rate was converted to cross sections and the emission angle in the laboratory into those in the centre of mass system.

4.1 π *production*

4.1.1 *Experimental findings*: For the π-production very close to threshold isotropic angular distributions are observed [4]. For higher beam momenta the angular distribution becomes backward peaked for the heavy recoil. For a beam of 750 MeV/c it has an almost exponential slope.

For higher beam momenta an almost isotropic component shows up for forward scattering with growing importance with increasing beam momentum. This can be seen from figure 5 which shows angular distributions for ^{3}He ions in the centre of mass system. The data up to 850 MeV/c are published in [6], the other data are preliminary. One point measured at $\cos(\theta) = -1$ which corresponds to zero degree in the laboratory was measured with the magnetic spectrograph BIG KARL.

In figure 6 we compare the present data with earlier results.

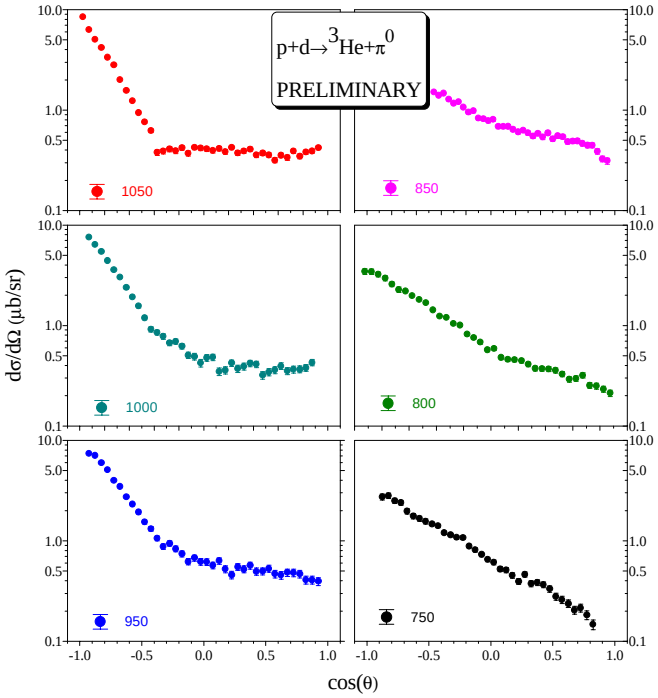

Figure 5. Angular distributions of the recoiling ^{3}He ions from the $pd \to {}^3\mathrm{He}\pi^0$ reaction for beam momenta given next to the appropriate data set.

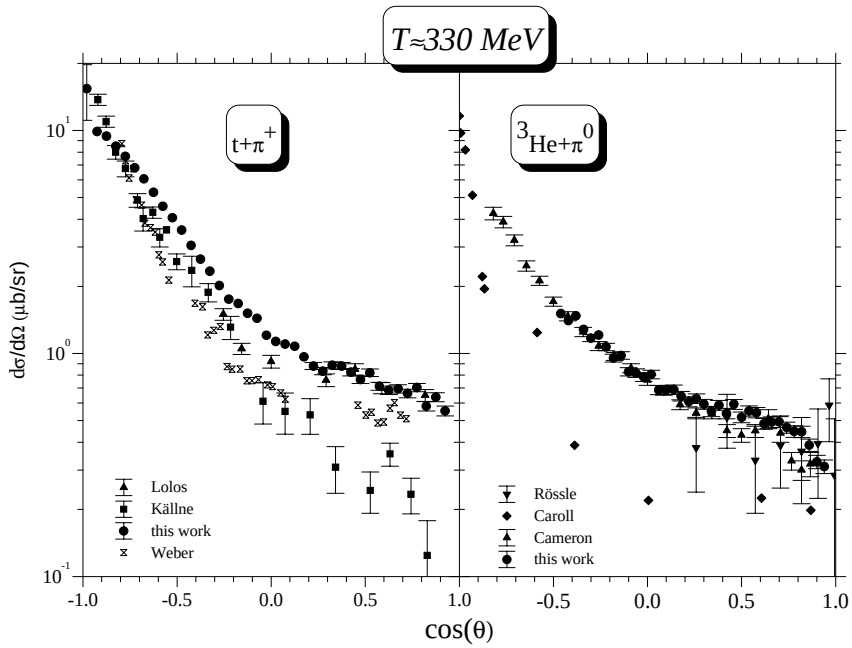

Figure 6. Comparison of the present results for neutral and charged pion production with earlier data from [5,7,8] for π^0 production and from ref. [9–11] for the π^+ production. The data correspond to bombarding energies in an interval 330 MeV to 350 MeV.

For the π^+ production, where our data for this beam energy are more complete than for π^0 production, the present data are larger than the other data especially for forward scattering where the cross section is small. The data from Weber *et al* [7] and Lolos *et al* [8], although much smaller than our data, show the onset of the isotropic component, while the data set from Källne *et al* [5] falls off almost exponentially. For the π^0 production the data from [10] are off the other data points. The data from Rössle *et al* [11] are from the isospin related $nd \to t\pi^0$ reaction. They show large error bars due to poor statistics. The data set from Cameron *et al* [9] is in good agreement with the present data.

In order to extract total cross sections we fitted Legendre polynomials to the angular distributions:

$$\frac{\mathrm{d}\sigma(\cos(\vartheta))}{\mathrm{d}\Omega} = \sum_l A_l P_l(\cos(\vartheta)) \tag{1}$$

with A_l the fit coefficients. The total cross section is given by

$$\sigma = 4\pi A_0. \tag{2}$$

We found that polynomials up to $l = 5$ contribute. The lions share to the forward backward asymmetry comes from $l = 1$. In figure 7 we show the momentum dependence of the presently deduced values of A_1 and compare it with other data. In order to become

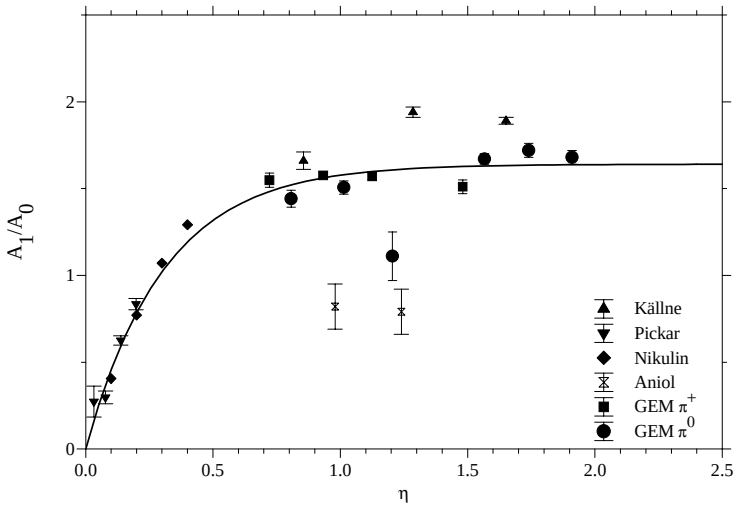

Figure 7. Dependence of the ratio of Legendre coefficients as function of the dimensionless pion centre of mass momentum. The earlier data are from refs [4,5,12,13]. The solid curve is to guide the eye.

independent of possible uncertainties in the absolute cross section we perform the comparison on a relative base, i.e. we show the ratio A_1/A_0 as function of the dimensionless pion centre of mass momentum $\eta = p_\pi/m_\pi$.

One point from the present measurement falls off the band formed by the present data. It corresponds to π^0 production at 850 MeV/c, where the angular distribution is truncated (compare figures 5 and 6). This is even more the case for two measurements at the largest beam momenta for π^0+ production, which are, therefore, not shown in the figure. The same may be true for the data from [12]. Only a few points (6 and 8) contribute to the angular distributions. The reaction really studied was $\pi^- + {}^3\mathrm{He} \to d + n$. Legendre polynomial fits to only second order were performed. It was already pointed out in [12] that this angular distribution is different from the one from $p + d \to {}^3\mathrm{H} + \pi^+$ reactions. The data disagree with those from [5] for the same reaction. We have fitted a smooth curve to our data plus those in the near threshold region. It is also shown in the figure to guide the eye.

4.1.2 *Models for pion production:* In order to avoid ambiguities we restrict the discussion on π^+ production. It is straightforward to apply all aspects to π^0 production. Since the pioneering paper of Ruderman [14] the reaction

$$p + d \to {}^3\mathrm{H} + \pi^+ \tag{3}$$

is related to the elementary nucleon–nucleon reaction

$$p + p \to d + \pi^+, \tag{4}$$

treating the additional neutron in the target deuteron as a spectator. The graph of this reaction is shown in the upper left part of figure 8. Besides trivial kinematical and spin factors

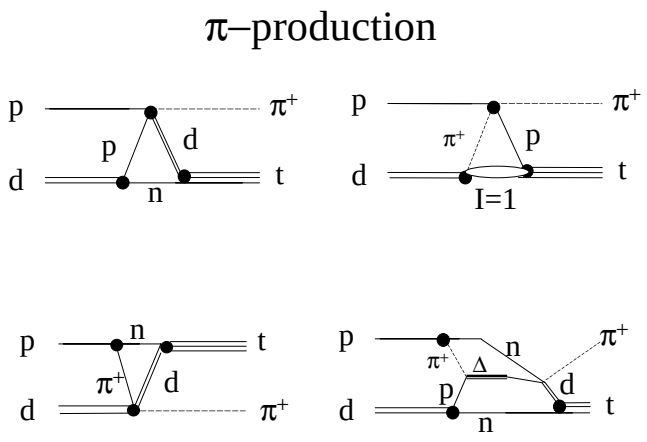

Figure 8. Upper left: Quasi–free (knock on) production. Upper right: One pion exchange. The intermediate 'd' has to be in an isospin $I = 1$ state. For a real intermediate deuteron the exchanged meson has to be an isoscalar one like $\eta,\ \rho, \ldots$. Lower left: One pion exchange with scattering of this pion on the deuteron. Lower right: Microscopic view of knock on graph with an intermediate Δ resonance excitation.

the cross section (or the corresponding amplitudes) and a form factor enter. The latter are indicated by the dots. This graph is treated in various depths of sophistication by different authors. Barry [15] in a relativistic treatment used Gaussians for both the deuteron and the triton wave functions, more precisely the $n - d$ component of the triton wave function. Comparison with pion forward angle data showed the need for a rather large triton distribution, wider than the deuteron. Locher and Weber [16] applied also a cluster wave function for the triton and a Hulthén wave function for the deuteron. The parameters for both functions were chosen to fit the respective charge form factor. This approach is an effective one, since only spin averaged quantities enter. This is especially true for the deuteron wave function. The s-state has a minimum around $q \approx 2.1/\text{fm}$. The Hulthén function at this momentum thus accounts for only the d-state of the deuteron. Germond and Wilkin [17] employed sums of exponentials as cluster wave functions, but for s-waves and d-waves separately. This model also allows to predict polarization observables similar as in the model by Falk [18]. Fearing [19] introduced in addition multiple scattering. The distortions in both the entrance and exit channel modify the absolute cross section but not the shape of the angular distributions. A more detailed discussion can be found in ref. [1].

The one pion exchange graph figure 8 requires an intermediate 'deuteron' in an isospin 1 state or the exchange of an isoscalar meson. This graph has never been calculated. The next graph is the pion rescattering on the deuteron. It should be effective at pion backward angles. Barry [15] calculated the corresponding cross section employing elastic $\pi d \rightarrow d\pi$ cross sections. Locher and Weber [16] made use of the connection of this graph to the direct one via the Pauli principle. This ansatz allows the coherent sum of both processes. Also the reactions with an unbound np-pair instead of a deuteron are included via antisymmetrization. This can be seen from the last graph in figure 8, which is a microscopic description of the knock-on term with an intermediate Δ excitation.

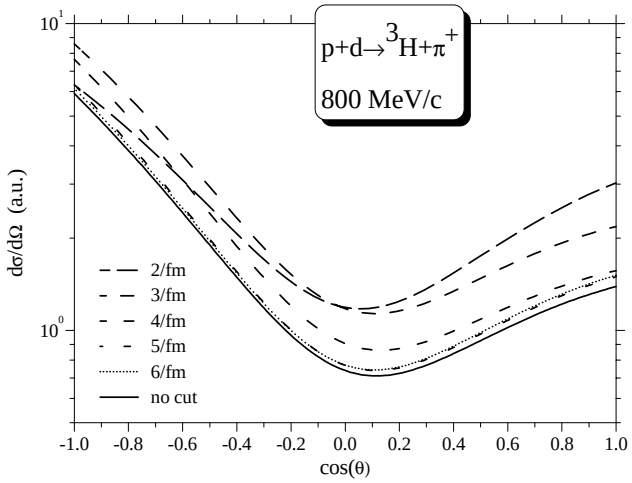

Figure 9. The sensitivity of the differential cross section to the momentum range of the integration of the form factors.

Ueda [20] attacked the problem by splitting the many-body process into coupled multi-, three-, and two-body systems which were treated in a relativistic and unitary approach. Numerical input is obtained by adjusting potential parameters to two body scattering amplitudes: $NN - NN$, $NN - d\pi$, $\pi d - \pi d$, $NN - N\Delta$, $\pi d - N\Delta$, and $N\Delta - N\Delta$.

To overcome the limitations and to challenge the validity of the 'deuteron' approaches, more microscopic models have been suggested [1,21,22]. Kingler [23] has extended the model originally developed for pion production [22] to include higher-resonances. The original model was limited to only pion exchange, Δ resonance excitation as well as non resonant contributions. The extension treats other meson exchanges as well as higher baryon resonances than the Δ. The vertex function for the different baryon–baryon–meson couplings were calculated in a simple quark model and are momentum dependent.

4.1.3 *Model comparison:* In the following we will concentrate on data comparison against calculations within the Locher–Weber model [16]. The elementary process $pp \rightarrow d\pi^+$ occurs in the reaction off-shell. This imports some ambiguities how to treat the effective energy and momentum in the $pp \rightarrow d\pi^+$ subamplitude. As limiting cases one can treat the internal deuteron on the mass shell. In this case the Δ resonance bump occurs at a proton energy of 450 MeV. If the internal proton is on the mass shell the bump occurs at 600 MeV. Here we have chosen the same pion centre of mass momentum in both reactions, which is different than the original approach. We used also the same centre of mass scattering angle for the pion in both systems. Locher and Weber [16] used a rather old parameterization of the differential $pp \rightarrow d\pi^+$ cross sections restricted to a term $\propto \cos^2(\theta)$. We fitted Legendre polynomials to all recent data and fitted smooth curves to the momentum dependencies of the Legendre coefficients.

As examples the data are compared with several model calculations also shown in figures 10 and 11. Here, we restrict ourselves to comparisons with published calculations for beam momenta close to the present ones or perform such calculations in the very transparent

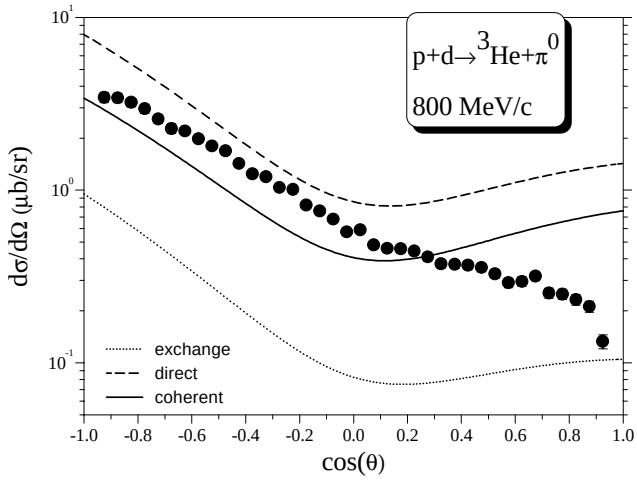

Figure 10. Comparison of the direct production and the exchange term. The solid curve is the coherent sum of both contributions.

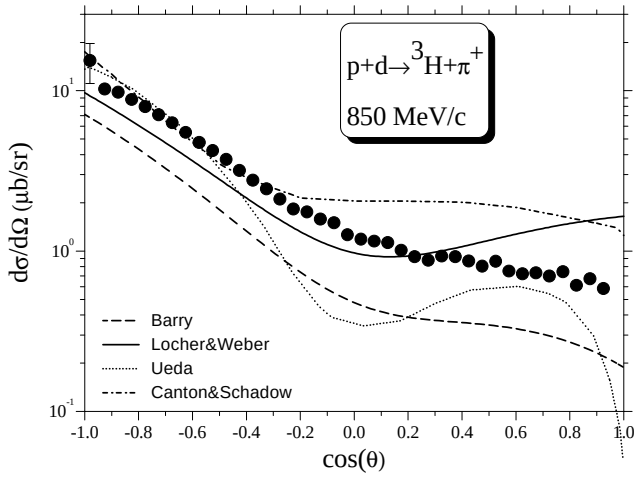

Figure 11. Angular distribution for pion emission for the reaction $pd \rightarrow {}^3\mathrm{H}\pi^+$ at a beam momentum of 850 MeV/c. The curves are calculations from [1,16,20].

Locher–Weber model [16]. The differential cross section in this model is given by

$$\frac{\mathrm{d}\sigma}{\mathrm{d}\Omega} = S\ K\,|F_D(q) - F_E(q)|^2\,\frac{\mathrm{d}\sigma}{\mathrm{d}\Omega}(pp \rightarrow d\pi^+) \tag{5}$$

with S, a spin factor, K, a kinematical factor, and F_D, the direct form factor and F_E, the

exchange form factor, i.e. an elastic πd scattering after pion emission from the incident proton. The form factors were evaluated with emphasis on the short range–components of the deuteron and the triton. This is achieved by fitting the free parameters in a Hulthén function to the deuteron–charge form factor and similarly for tritium (more precisely the wave function of the spectator neutron relative to the deuteron), the parameters for the Eckart function to the tritium-charge form factor.

In order to test the sensitivity of the calculations on the momentum interval in the wave function we introduced step functions in the integrals of the form factors, thus limiting the range of momenta. Angular distributions with different maximal momentum transfer are shown in figure 12.

Too small momentum transfer leads to too large cross sections. If the range exceeds 6 fm^{-1} the result becomes independent on truncation. In other words: the present result is sensitive to large momentum transfers up to 6 fm^{-1} or 1200 MeV/c. This is much more than the mean momentum transfer of ≈350 MeV/c discussed in the introduction. It can be further seen from figure 12 that the interference between direct and exchange term is different for forward and backward angles. To study this effect in more detail we show these two contributions as well as their coherent sum in figure 9. It becomes evident from this comparison that the exchange term is less important at this beam momentum than the direct term. However, for larger beam momenta the exchange term increases. For 1000 MeV/c it is almost one half of the direct term for the backward angles. Also shown in figure 9 are the present data. The calculation underestimates the backward cross sections and overestimates the forward cross section largely. The calculations do not show the same slope in this range as the data. This calculation was performed without any additional normalization, i.e. the wave function were normalized to 1 [16].

All other calculations shown in figure 10 need normalization factors when compared to the data. The calculation from [20] is multiplied by 0.01, the one from [1] by 2. Using this factor the total cross section as almost the experimental one. Without this normalization the

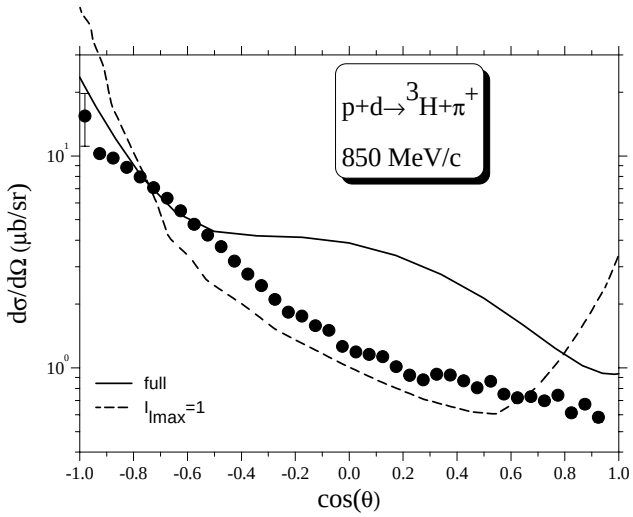

Figure 12. Same as figure 11, but for calculations within the microscopic model [23].

range with large momentum transfer is better reproduced. We also studied the functional behaviour given by Barry [15], i.e. Gaussians for both the deuteron and the spectator neutron in the triton wave functions. A very large width of the triton wave function of 370 MeV/c had to be applied in order to account for the data. This has to be compared with 87 MeV/c for the deuteron, which makes the approach suspicious. For larger beam momenta local minima show up which are not in the data. The origin of such dips may be an artefact of non proper symmetrization of the wave function [19]. Similarly the local minimum at $\cos(\theta) \approx 0$ for 850 MeV/c in Ueda's calculation is not supported by the data. In figure 11 we compare the present data with calculations in the microscopic model from [22,23]. For this calculation π and ρ exchange were found to be equally important. Resonances only up to the Δ contribute. The solid curve is the coherent sum of all processes while the dashed curve is the contribution of angular momenta only up to 1. For the intermediate states the closure approximation was applied and the nuclei are approximated by shells with an oscillator strength of 1.8 fm, adjusted to the height of the data. The local maximum around $\cos(\theta) \approx 0$ is not in the data. It may be due to the momentum dependence of the vertex functions employed. In calculations for the $pp \to d\pi^+$ reaction a similar dependence was found. It vanished if the vertex functions from [22] were applied.

This range with large momentum transfer is rarely reproduced by a calculation. Green and Sainio [21] even claim their calculations to be unreliable in this range. The large and almost exponential shaped component may be attributed to the direct production graph. Therefore, new physics may be hidden in the small more isotropic component.

4.2 η *production*

4.2.1 *Experimental results*: We have studied η production at a beam momentum of 1673 MeV/c. Two runs were made where the first run called run A suffered from unfavourable beam conditions. In contrast to pion production one is here dealing with a substantial background due to multi-pion production. The peak to background ratio is typically 2 to 1. We have fitted smooth curves plus a Gaussian to the missing mass spectra for the different angle intervals yielding the angular distribution shown in figure 13. The data are from different runs which agree well with each other. More details on the data evaluation is given elsewhere [24]. The present data were complemented by two points from the literature [25,26]. The present angular distribution seems to be dominated by p-wave in contrast to near threshold, where the angular distributions are s-wave dominated [27]. A Legendre polynomial of second order was found to account for the data and extract the total cross section.

4.2.2 *Model comparison*: Similarly to the case of pion production different graphs can contribute to η production. Such graphs are shown in figure 14. The upper row shows η production in one pion exchange with and without excitation of nucleon resonances. The only resonance known to couple strongly to the η-nucleon channel is the S_{11} resonance $N^*(1535)$. However, two step processes as shown in the lower row may be also important. This is supported by the large momentum transferred in the reaction, making one and two body processes unlikely [28]. Similar findings were reported by Fäldt and Wilkin [29] applying the two step model to threshold data. The same graph was calculated in terms of the on-shell amplitude by Kilian and Nann [30]. We have compared the corresponding calculation normalized to data. This model cannot account for the data.

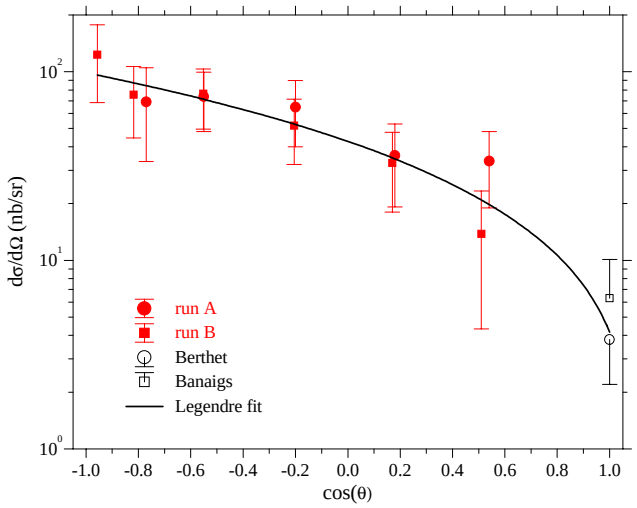

Figure 13. Angular distribution of ^{3}He in η production in the cm system. The two different runs are indicated by the indicated symbols. Two points from the literature are added [25,26]. The solid curve indicates a Legendre polynomial fit.

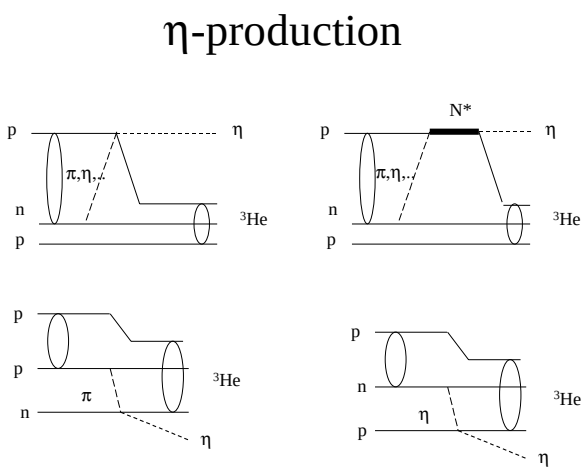

Figure 14. Graphs for η production. Upper left: one meson exchange. Upper right: one meson exchange with excitation of an intermediate nucleon resonance. Lower left: two step process: the intermediate pion scatters on the third nucleon. Lower right: two step process with an elastic η-nucleon scattering.

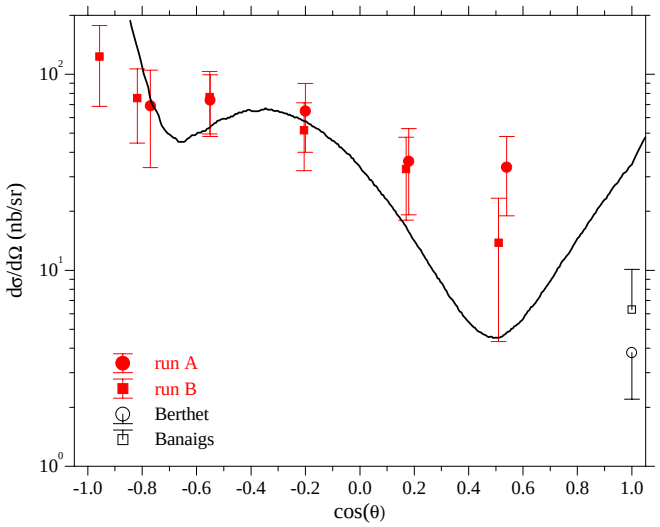

Figure 15. Angular distribution of η production in the cm system. Two points from the indicated references are added [25,26]. The solid curve is from a model calculation [23].

Kingler [23] has also calculated the present reaction. The largest contribution to the cross section comes from the $NN\rho$ and $NN\omega$ interactions while the contribution due to $NN^*(1535)\pi$ interaction is one order of magnitude smaller. The contributions of other resonances like $N^*(1440)$, $N^*(1650)$, and $N^*(1710)$ are even smaller. However, the form factor is calculated only for harmonic oscillator wave functions with the frequency being a free parameter varied to fit the experimental data. The model predictions are tested against the differential data in figure 15. Obviously, the calculation shows structures not observed in the present data.

From the Legendre polynomial fit to the angular distribution a total cross section of $\sigma = 573 \pm 83\ (\mathrm{stat.}) \pm 69\ (\mathrm{syst.})\ nb$ was deduced. This result is close to the one obtained by Banaigs *et al* [25] at a slightly higher energy. All cross section from threshold up to $T_p \approx 1500$ MeV, shown in figure 16, could be nicely accounted by a simple calculation. This energy region corresponds to the centre of the $N^*\ S_{11}$ resonance ($\Gamma \sim 200$ MeV) known to couple strongly to the η–N channel [31]. One may therefore attempt to describe the cross section by an intermediate $N^*(1535)$ resonance excitation:

$$\sigma(E) = \frac{p_\eta}{p_p}|M(E)|^2 \tag{6}$$

with E the excitation energy and M the matrix element which is calculated as in photoproduction on the proton [32] as Breit–Wigner form with an energy dependent width. All parameters were taken from [32] and [31].

The only free parameter is the strength fitted to the present data point. The trend of the data is reproduced, which may be taken as an indication that production of the $N^*(1535)$

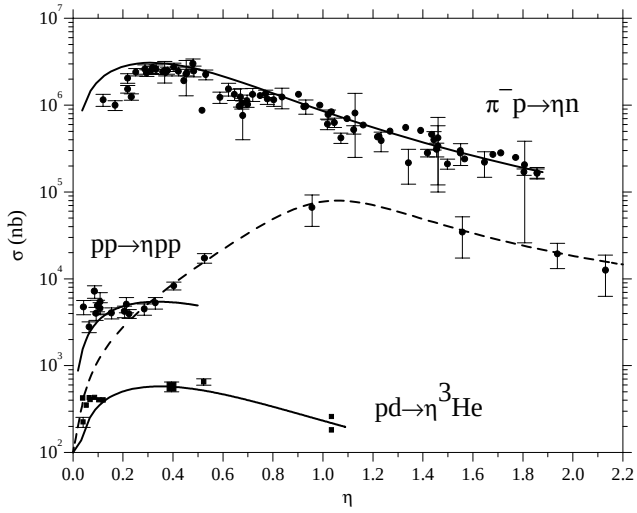

Figure 16. Excitation functions of η production in different reactions as function of $\eta = p^*_\eta / m_\eta$. The upper band is the data from $\pi^- p \to n\eta$ reactions, the middle band from $pp \to pp\eta$ reactions and the lowest one from $pd \to {}^3\mathrm{He}\eta$ reactions. The solid curves are predictions assuming the matrix element from photoproduction of η mesons off the proton assuming only resonance production of the $N^*(1535)$. For the $pp \to pp\eta$ reaction an additional resonance at 1740 MeV/c was assumed (dashed curve).

resonance is the dominant reaction mechanism and that the product of kinematics and form factor changes only very little over the present energy range. The path

$$p + p \to \pi^+ + d \tag{7}$$

$$\pi^+ + n \to N^* \to \eta + n \tag{8}$$

with the final fusion

$$n + d \to {}^3\mathrm{He} \tag{9}$$

is larger by isospin considerations than the reaction with an initial $np \to d\pi^0$ or $pp \to d^*\pi^+$. A large fraction of the total momentum transfer is transferred to the vertex 8. Therefore, nuclear form factors do not suppress the cross section, which explains the success of the simple model.

Deviations occur near threshold which might be an indication of strong final state interactions.

5. Isospin

Isospin is known to be only an approximate symmetry. Trivial effects like Coulomb interaction break this symmetry. However, isospin symmetry breaking will occur when the up and down quark masses are different. Differences in the quark masses lead to $\pi^0 - \eta$

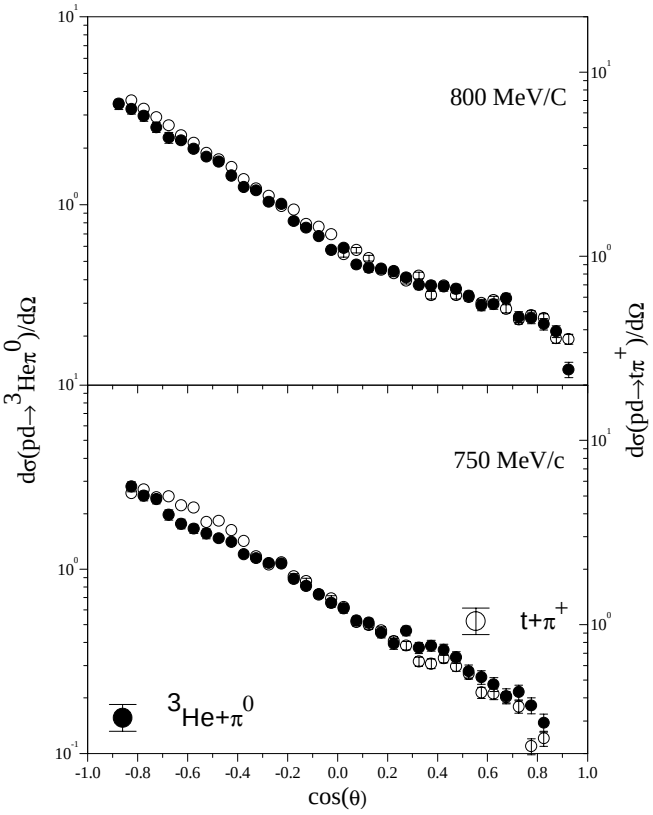

Figure 17. Angular distribution for the two reactions $pd \rightarrow t\pi^+$ (right axis) and $pd \rightarrow {}^3\mathrm{He}\pi^0$ (left axis) and for beam momenta of 750 MeV/c and 800 MeV/c. The data for $pd \rightarrow t\pi^+$ reaction are corrected for Coulomb effects.

mixing [33]. This mixing affects π^0 production in contrast to π^+ production. One may expect a deviation of the ratio

$$R(\theta) = \frac{\mathrm{d}\sigma(\theta, pd \rightarrow t\pi^+)}{\mathrm{d}\sigma(\theta, pd \rightarrow {}^3\mathrm{He}\pi^0)} \tag{10}$$

from 2 which is the ratio according to the Clebsch–Gordan coefficients. The present experiment has the advantage to measure both reactions simultaneously, thus avoiding a number of possible uncertainties which cancel. On the other hand the proper scale for such comparison is not known. Close to threshold large deviations show up whether a comparison is made for the same centre of mass pion momentum or η which is the same quantity divided by the pion mass, excess energy or momentum transfer. Here we compare differential cross sections for the two reactions for beam momenta of 750 and 800 MeV/c, respectively (see figure 17).

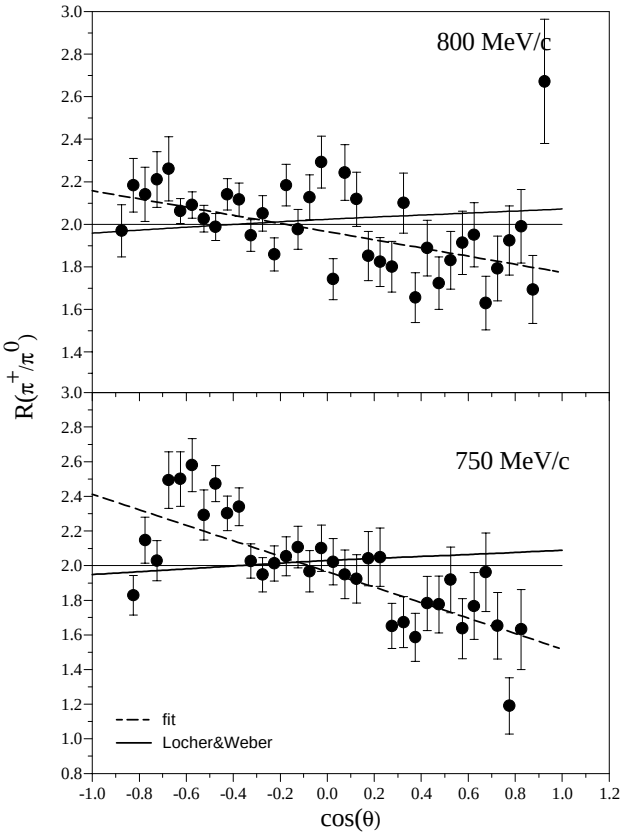

Figure 18. The ratio eq. (10) as function of the scattering angle. The isospin Clebsch–Gordan result 2 is also shown. The dashed line is a fit to the data in order to guide the eye. The solid line is the prediction of the Locher–Weber model [16].

The charged exit channel is corrected for the Coulomb effect by a simple Gamow factor. The left and right y-axis scalings differ by a factor of two. It can be seen that the cross section for the charged pion production is slightly larger than the one for neutral pion production. The effect is more pronounced when the ratio is directly inspected. This is done in figure 18. The deduced values for the ratios scatter around 2. The tendency to change this value with respect to momentum transfer is indicated in the figure by straight lines. Also shown is the prediction within the Locher–Weber model [16], where we have assumed an isospin two ratio for the elementary reactions $pp \to d\pi^+$ and $pn \to d\pi^0$.

Similar deviations from the simple factor of 2 have been obtained, when the ratio is performed for the matrix elements as function of the four momentum transfer t [6]. The matrix elements show dependencies on both Mandelstam variables t and s, the total energy squared.

References

[1] L Canton, G Cattapan, G Pisent, W Schadow and J P Svenne, *Phys. Rev.* **C57**, 1588 (1998)
L Canton and W Schadow, *Phys. Rev.* **C56**, 1231 (1997)
[2] M Betigeri *et al*, *Nucl. Instrum. Methods Phys. Res.* **A421**, 447 (1999)
[3] M Drochner *et al*, *Nucl. Phys.* **A643**, 55 (1998)
[4] V N Nikulin *et al*, *Phys. Rev.* **C54** 1732 (1996)
[5] J Källne, J E Bolger, M J Devereaux and S L Verbeck, *Phys. Rev.* **24**, 1102 (1981)
[6] M Betigeri *et al*, *Nucl. Phys.* **A** (in press)
[7] P Weber *et al*, *Nucl. Phys.* **A534**, 541 (1991)
[8] G J Lolos *et al*, *Nucl. Phys.* **386**, 477 (1982)
[9] J M Cameron *et al*, *Nucl. Phys.* **A472**, 718 (1987)
[10] J Caroll *et al*, *Nucl. Phys.* **A305**, 502 (1978)
[11] M Dutty, Diploma thesis, Freiburg 1981 and E Rössle *et al*, *Proc. Conf. on Pion Production and Absorption in Nuclei* edited by R D Bent, *AIP Conf. Proc.* **79**, 171 (1982)
[12] K A Aniol *et al*, *Phys. Rev.* **C33**, 1714 (1986)
[13] M A Pickar *et al*, *Phys. Rev.* **C46**, 397 (1992)
[14] M Ruderman, *Phys. Rev.*, **87**, 383 (1952)
[15] G W Barry, *Phys. Rev.* **D7**, 1441 (1973)
[16] M P Locher and H J Weber, *Nucl. Phys.* **B76**, 400 (1974)
[17] J-F. Germond and C Wilkin, *J. Phys.* **G14**, 181 (1988); **G16**, 381 (1990)
[18] W R Falk, *Phys. Rev.* **C50**, 1574 (1994); **C61**, 034005 (2000)
[19] H W Fearing, *Phys. Rev.* **C16**, 313 (1977)
[20] T Ueda, *Nucl. Phys.* **A505**, 610 (1974)
[21] A M Green and M E Sainio, *Nucl. Phys.* **A329**, 477 (1979)
[22] M Harzheim *et al*, *Z. Physik* **340**, 399 (1991)
[23] J Kingler, Ph.D Thesis (Univ. Bonn, 1995); and private communications to H.M.
[24] M Betigeri *et al*, *Phys. Lett.* **B472**, 267 (2000)
[25] J Banaigs *et al*, *Phys. Lett.* **B45**, 394 (1973)
[26] P Berthet *et al*, *Nucl. Phys.* **C443**, 589 (1985)
[27] B Mayer *et al*, *Phys. Rev.* **C53**, 2068 (1996)
[28] J M Laget and J F Lecolley, *Phys. Rev. Lett.* **61**, 2069 (1988)
[29] G Fäldt and C Wilkin, *Nucl. Phys.* **A587**, 769 (1995)
[30] K Kilian and H Nann, *AIP Conf. Proc.* **221**, 185 (1990)
[31] C Caso *et al*, Particle Data Group, *The European Phys. J.* **3**, 1 (1999)
[32] B Krusche, *Acta Phys. Polonica* **B27**, 3147 (1996)
[33] A Magiera and H Machner, *Nucl. Phys.* **A674**, 515 (2000)